







# Large Models for Cooperative Control of Connected and Autonomous Vehicles

Xin Wang, *Member, IEEE*, Jianhui Lyu , *Member, IEEE*, Adam Slowik , *Senior Member, IEEE*, J. Dinesh Peter , *Member, IEEE*, Byung-Gyu Kim , *Senior Member, IEEE*, B. D. Parameshachari , *Senior Member, IEEE*, and Keqin Li , *Fellow, IEEE*

**Abstract**—Integrating large models (LMs) into future vehicles and transportation systems marks a significant advancement in mobility and transportation technology. Incorporating artificial intelligence and machine learning, these LMs are poised to revolutionize various aspects of transportation. This paper proposes LMs-based approaches for cooperative control and coordination of connected and autonomous vehicle (CAV) fleets. Specifically, algorithms based on the alternating direction method of multipliers (ADMM) are developed for distributed optimization of CAV trajectories. The synchronous ADMM and asynchronous ADMM algorithms enable parallelized coordination of large-scale CAV systems. Simultaneously, we propose a distributed training scheme where each CAV trains its cost and dynamics networks on simulators local to each vehicle. A central coordinator interacts with the vehicles to tune the coupling networks. Then, we introduce an innovative car-following model named the integrated velocity and acceleration fusion model that integrates state information from multiple lead and following vehicles to determine the optimal acceleration for the subject CAV. While we utilize graph sample and aggregate –based neural network and the gated recurrent unit and propose a model for recognizing driving intentions and predicting the trajectories of surrounding vehicles based on these theories. Simulation results demonstrate enhanced traffic efficiency, safety, robustness, and scalability using LMs for cooperative control of CAV.

**Index Terms**—Large models, connected and autonomous vehicles, alternating direction method of multipliers, cooperative control, car-following.

Manuscript received 19 November 2023; revised 21 February 2024 and 3 May 2024; accepted 3 June 2024. Date of publication 5 June 2024; date of current version 14 February 2025. This work was supported by the National Natural Science Foundation of China under Grant 62202247. The review of this article was coordinated by the Guest Editors of the Special Section on Large Models for Future Vehicles and Transportation. (*Corresponding author: Jianhui Lyu.*)

Xin Wang is with Northeastern University, Shenyang 110819, China, and also with Dongneng (Shenyang) Energy Engineering Technology Company Ltd., Shenyang 110819, China (e-mail: dnsy\_heinrich@neueet.com).

Jianhui Lyu is with Peng Cheng Laboratory, Shenzhen 518057, China (e-mail: lvjianhui2012@163.com).

Adam Slowik is with the Koszalin University of Technology, 75-453 Koszalin, Poland (e-mail: adam.slowik@tu.koszalin.pl).

J. Dinesh Peter is with the Karunya Institute of Technology and Sciences, Tamil Nadu 641 114, India (e-mail: dineshpeter@gmail.com).

Byung-Gyu Kim is with the Sookmyung Women's University, Seoul 04310, Republic of Korea (e-mail: bg.kim@sookmyung.ac.kr).

B. D. Parameshachari is with the Nitte Meenakshi Institute of Technology, Bengaluru, Karnataka 560064, India (e-mail: paramesh@nmit.ac.in).

Keqin Li is with the State University of New York, New Paltz, NY 12561 USA (e-mail: lik@newpaltz.edu).

Digital Object Identifier 10.1109/TVT.2024.3409890

## I. INTRODUCTION

CONNECTED and autonomous vehicles (CAVs), endowed with advanced sensing, communication, and control technologies, offer transformative potential for the future of transportation [1]. The primary advantages of CAVs include improved traffic flow, enhanced road safety, reduced congestion, lower emissions, and superior mobility services [2], [3], [4]. However, several complex challenges must be addressed to harness these benefits on a large scale fully. These challenges encompass perception, planning, control, and coordination within expansive transportation networks that include CAVs and human-driven vehicles (HDVs), pedestrians, and various infrastructure components [5], [6]. Effectively integrating CAVs into this dynamic mix demands sophisticated solutions that can handle the complexities of real-world traffic environments and the diverse behaviors of different road users. Achieving this integration is crucial for creating more intelligent, responsive, sustainable transportation systems.

The advent of large models (LMs) based on deep neural networks and advanced distributed optimization algorithms have opened up novel avenues for addressing coordination challenges in transportation systems [7]. LMs, characterized by their vast number of parameters, often in the billions, are trained on extensive and diverse datasets [8], [9]. This training enables them to learn intricate functions, mapping inputs to outputs in ways that traditional analytical methods find challenging. Once pre-trained, these models are fine-tuned for specific tasks, making them highly adaptable and efficient. In transportation, LMs are particularly valuable for the cooperative control and coordination of CAVs. They offer a data-driven, optimization-based approach to managing large fleets of CAVs, aiming to enhance overall traffic flow and improve safety across the system [10]. This advancement is significant in intelligent transportation systems, where the dynamic interplay of numerous vehicles and infrastructure components presents a formidable challenge [11]. LMs thus stand as a promising solution, enabling more effective and safer traffic management in increasingly congested urban environments.

LMs, such as transformer-based LMs, have emerged as disruptive machine learning techniques, as exemplified by recent architectures like BERT and GPT [12], [13], [14]. Their promise for intelligent transportation systems stems from the innate ability to learn from vast datasets and adapt to diverse predictive

tasks crucial for managing traffic complexity. These models incorporate key innovations that capture intricate spatial and temporal dynamics. Leveraging such capabilities by training transformer-based large models on ever-growing transportation corpora allows learning highly complex traffic flow interactions. Transformer-based large model architectures provide a flexible modeling paradigm to encapsulate intricate transportation phenomena in data through scalable, self-attentive compositional representations. By capturing systemic dependencies and offering easy downstream adaptability, they promise to significantly advance intelligent systems for managing congestion, safety, and other challenges facing modern transportation.

Distributed optimization algorithms, particularly the consensus alternating direction method of multipliers (ADMM), play a pivotal role in enabling the application of LMs to multi-agent coordination challenges, such as those encountered in managing fleets of CAVs [15]. These algorithms facilitate decentralized optimization of vehicle trajectories, allowing each CAV to tackle a local sub-problem individually. Simultaneously, this approach is grounded in using specific cost functions and dynamics modeled by LMs, with the capability to reach a consensus on shared decision variables through dual variable updates among neighboring CAVs [16], [17], [18], [19]. This methodology effectively sidesteps the need for a central controller and the complexities associated with extensive vehicle-to-infrastructure coordination. When LMs are combined with ADMM-based distributed coordination algorithms, optimizing the trajectories of large-scale CAV fleets in real time becomes feasible.

In heterogeneous traffic environments where both CAVs and HDVs coexist, LMs bring a novel dimension to understanding the intricate dynamics of human driving behaviors [20], [21], [22]. These LMs can comprehensively capture the complexities of vehicle interactions and the psychology underpinning human driving actions. Consequently, they enable the synthesis of car-following and lane-changing models that closely mimic real-world traffic flow patterns, offering a more accurate representation of mixed traffic scenarios [23], [24]. Integrating information from multiple surrounding vehicles is a hallmark of LMs, empowering them to design sophisticated control strategies for CAVs. These strategies enhance traffic stability and effectively mitigate disturbances in the presence of diverse road users [25], [26], [27], [28], [29]. By leveraging the power of LMs, transportation systems can move closer to achieving a harmonious coexistence of autonomous and human-driven vehicles. Nonetheless, it is imperative to acknowledge that modeling heterogeneous multi-agent transportation systems poses challenges [23]. Scalability, reliability, and stability are foremost concerns that require careful consideration.

To summarize, incorporating LMs enabled by recent advances in computation power and dataset availability has significant potential to address complex coordination problems arising in CAV systems and mixed traffic environments. However, there remain essential research gaps related to: (i) Distributed optimization algorithms that can scale to large numbers of CAVs and enable real-time trajectory planning and coordination; (ii) Car-following models tailored to mixed traffic environments that leverage multi-vehicle information while ensuring string

stability; (iii) Validation of the benefits of LM-based control and coordination strategies through analysis and realistic traffic simulations.

This paper aims to develop LM-based methodologies to address these research gaps. The contributions include:

- 1) We present algorithms using ADMM for the distributed optimization of CAV trajectories, which are crucial for the efficient and effective management of vehicle movements in a connected environment.
- 2) We propose a distributed training scheme where each CAV trains its cost and dynamics networks on simulators local to each vehicle. A central coordinator interacts with the vehicles to tune the coupling networks.
- 3) We propose a novel car-following model named the integrated velocity and acceleration fusion (IVAF) model. This model merges state data from various leading and following vehicles to identify the best acceleration for the specific CAV.
- 4) We use graph neural network theory and the gated recurrent unit (GRU), proposing a model for recognizing driving intentions and predicting the trajectories of surrounding vehicles based on these theories.

The rest of this paper is structured as follows: Section II illustrates the system model, Section III studies the cooperative control of CAV, Section IV presents the simulations and results analysis, and Section V shows the conclusion.

## II. SYSTEM MODEL

We consider the problem of coordinating a fleet of  $N$  CAVs traveling on a roadway. The positions and velocities of the vehicles are coupled through inter-vehicle constraints such as collision avoidance and traffic flow constraints. The goal is to optimize the trajectories of the vehicles over a finite horizon to achieve objectives related to safety, efficiency, and ride comfort.

### A. Problem Formulation

The trajectory of each vehicle  $i \in \{1, \dots, N\}$  over the finite horizon is parameterized by the control inputs.

$$\mathbf{u}_i = [u_i(0), \dots, u_i(T_1 - 1)]^T. \quad (1)$$

where  $T$  is the horizon length and  $T_1$  is the control horizon. The system evolution is given by the discrete-time dynamics.

$$\mathbf{x}_i(t+1) = f_{\theta_i}(\mathbf{x}_i(t), \mathbf{u}_i(t)). \quad (2)$$

where  $\mathbf{x}_i$  is the state vector (position, velocity etc.), and  $f_{\theta_i}$  is a dynamics network with parameters  $\theta_i$ .

The centralized optimal control problem with coupled constraints is formulated as follows [30].

$$\begin{aligned} \min_{\mathbf{u}_1, \dots, \mathbf{u}_N} & \sum_{i=1}^N \left( l_i(\mathbf{x}_i, \mathbf{u}_i) + \sum_{j \in \mathcal{N}_i} c_{ij}(\mathbf{x}_i, \mathbf{u}_i, \mathbf{x}_j, \mathbf{u}_j) \right) \\ \text{s.t. } & \mathbf{x}_i(t+1) = f_i(\mathbf{x}_i(t), \mathbf{u}_i(t)), i = 1, \dots, N \\ & g_i(\mathbf{x}_i, \mathbf{u}_i) \leq 0, i = 1, \dots, N \\ & h_{ij}(\mathbf{x}_i, \mathbf{u}_i, \mathbf{x}_j, \mathbf{u}_j) = 0, (i, j) \in \mathcal{E}. \end{aligned} \quad (3)$$

where  $l_i$  is the stage cost for vehicle  $i$ ,  $c_{ij}$  are coupling costs between vehicles  $i$  and  $j$ ,  $\mathcal{N}_i$  is the set of neighbors of  $i$  based on the interaction topology,  $g_i$  are state and input constraints, and  $h_{ij}$  are coupling equality constraints such as collision avoidance.  $\mathcal{E}$  represents the edge set of the interaction topology graph.

Considering the large models for future vehicles and transportation, the overall cost function is as follows.

$$J(\mathbf{X}, \mathbf{U}) = \sum_{i=1}^N l_{\phi_i}(\mathbf{x}_i, \mathbf{u}_i) + \sum_{(i,j) \in \mathcal{E}} c_{\psi_{ij}}(\mathbf{x}_i, \mathbf{u}_i, \mathbf{x}_j, \mathbf{u}_j). \quad (4)$$

where  $l_{\phi_i}$  and  $c_{\psi_{ij}}$  are individual and coupling cost networks with parameters  $\phi_i, \psi_{ij}$ .

The constraints are represented implicitly by penalty terms in the cost:

$$l_{\phi_i}(\mathbf{x}_i, \mathbf{u}_i) = l^0 \phi_i(\mathbf{x}_i, \mathbf{u}_i) + \lambda g_{\omega_i}(\mathbf{x}_i, \mathbf{u}_i) c_{\psi_{ij}}(\mathbf{x}_i, \mathbf{u}_i, \mathbf{x}_j, \mathbf{u}_j) = c_{\psi_{ij}}^0(\mathbf{x}_i, \mathbf{u}_i, \mathbf{x}_j, \mathbf{u}_j) + \mu h_{\gamma_{ij}}(\mathbf{x}_i, \mathbf{x}_j). \quad (5)$$

where  $g_{\omega_i}$  and  $h_{\gamma_{ij}}$  represent state, input and coupling constraints, and  $\lambda, \mu$  are penalty weights.

The objective combines individual stage costs and coupling costs over the horizon length  $T$ . The dynamics constraints couple the states over time. The inequality constraints  $g_i$  enforce state and input limits for each CAV. The coupling equality constraints  $h_{ij}$  model interactions between CAVs such as collision avoidance.

To be more specific about the objective function, we define:

$$\sum_{t=0}^T l_{\phi_i}^t(\mathbf{x}_i(t), \mathbf{u}_i(t)). \quad (6)$$

$$l_{\phi_i}^t(\mathbf{x}_i(t), \mathbf{u}_i(t)) = (\mathbf{x}_i(t) - \mathbf{x}_i^{ref}(t))^T Q_i(\mathbf{x}_i(t) - \mathbf{x}_i^{ref}(t)) + \mathbf{u}_i(t)^T R_i \mathbf{u}_i(t). \quad (7)$$

where  $\mathbf{x}_i^{ref}$  is the reference trajectory for CAV  $i$ , and  $Q_i, R_i$  are weighting matrices. This quadratic stage cost penalizes deviation from the reference path.

The coupling costs are defined as follows.

$$c_{\psi_{ij}}(\mathbf{x}_i, \mathbf{u}_i, \mathbf{x}_j, \mathbf{u}_j) = \sum t = 0^{T-1} c_{\psi_{ij}}^t(\mathbf{x}_i(t), \mathbf{u}_i(t), \mathbf{x}_j(t), \mathbf{u}_j(t)). \quad (8)$$

where  $c_{\psi_{ij}}^t$  penalizes proximity between CAV  $i$  and  $j$  at time  $t$  to encourage collision avoidance.

The state and input constraints are as follows.

$$g_{\omega_i}^x(\mathbf{x}_i) = \mathbf{x}_i^{\min} \leq \mathbf{x}_i \leq \mathbf{x}_i^{\max}. \quad (9)$$

$$g_{\omega_i}^u(\mathbf{u}_i) = \mathbf{u}_i^{\min} \leq \mathbf{u}_i \leq \mathbf{u}_i^{\max}. \quad (10)$$

These define safety limits on states like positions and velocities as well as actuator limits on inputs like accelerations.

The coupling collision avoidance constraints [31] are as follows.

$$h_{\gamma_{ij}}(\mathbf{x}_i, \mathbf{x}_j) = |p_i - p_j|^2 - d_{safe}^2 \leq 0. \quad (11)$$

where  $p_i, p_j$  are the positions of CAV  $i$  and  $j$ , and  $d_{safe}$  is the safe distance threshold. This constrains the distance between vehicles above a safety margin.

## B. Constraint Convexification

The non-convexity in the above problem arises from the nonlinear dynamics  $f_i$  and constraints  $g_i, h_{ij}$ . We approximate these nonlinear functions by linearizing them about a nominal trajectory  $\bar{\mathbf{x}}_i, \bar{\mathbf{u}}_i$  for each CAV  $i$ :

$$\mathbf{x}_i(t+1) \approx A_i(t) \mathbf{x}_i(t) + B_i(t) \mathbf{u}_i(t). \quad (12)$$

$$g_{\omega_i}(\mathbf{x}_i, \mathbf{u}_i) \leq G_i \mathbf{x}_i + H_i \mathbf{u}_i \leq b_i. \quad (13)$$

$$h_{\gamma_{ij}}(\mathbf{x}_i, \mathbf{u}_i, \mathbf{x}_j, \mathbf{u}_j) \approx P_{ij}(t) \mathbf{x}_i + Q_{ij}(t) \mathbf{x}_j + R_{ij}(t) \mathbf{u}_i + S_{ij}(t) \mathbf{u}_j = 0. \quad (14)$$

where  $A_i, B_i, G_i, H_i$  and  $P_{ij}, Q_{ij}, R_{ij}, S_{ij}$  are obtained by linearizing the nonlinear functions about the nominal trajectory.

Specifically, the linearized discrete-time dynamics are obtained via:

$$A_i(t) = \frac{\partial f_{\theta_i}}{\partial \mathbf{x}}(\bar{\mathbf{x}}_i(t), \bar{\mathbf{u}}_i(t)). \quad (15)$$

$$B_i(t) = \frac{\partial f_{\theta_i}}{\partial \mathbf{u}}(\bar{\mathbf{x}}_i(t), \bar{\mathbf{u}}_i(t)). \quad (16)$$

The linearized state and input constraints are:

$$G_i = \nabla \mathbf{x} g_i(\bar{\mathbf{x}}_i, \bar{\mathbf{u}}_i). \quad (17)$$

$$H_i = \nabla \mathbf{u} g_i(\bar{\mathbf{x}}_i, \bar{\mathbf{u}}_i). \quad (18)$$

And the linearized coupling constraints are:

$$\begin{aligned} P_{ij}(t) &= \nabla \bar{\mathbf{x}}_i h_{\gamma_{ij}}(\bar{\mathbf{x}}_i(t), \bar{\mathbf{u}}_i(t), \bar{\mathbf{x}}_j(t), \bar{\mathbf{u}}_j(t)) \\ Q_{ij}(t) &= \nabla \bar{\mathbf{x}}_j h_{\gamma_{ij}}(\bar{\mathbf{x}}_i(t), \bar{\mathbf{u}}_i(t), \bar{\mathbf{x}}_j(t), \bar{\mathbf{u}}_j(t)) \\ R_{ij}(t) &= \nabla \bar{\mathbf{u}}_i h_{\gamma_{ij}}(\bar{\mathbf{x}}_i(t), \bar{\mathbf{u}}_i(t), \bar{\mathbf{x}}_j(t), \bar{\mathbf{u}}_j(t)) \\ S_{ij}(t) &= \nabla \bar{\mathbf{u}}_j h_{\gamma_{ij}}(\bar{\mathbf{x}}_i(t), \bar{\mathbf{u}}_i(t), \bar{\mathbf{x}}_j(t), \bar{\mathbf{u}}_j(t)). \end{aligned} \quad (19)$$

This convexifies the constraints, yielding a linear time-varying model for each CAV:

$$\mathbf{x}_i(t+1) = A_i(t) \mathbf{x}_i(t) + B_i(t) \mathbf{u}_i(t). \quad (20)$$

The linearized coupling constraints are written compactly as:

$$\mathbf{H}_{ij}(t) \mathbf{z}_i(t) + \mathbf{J}_{ij}(t) \mathbf{z}_j(t) = 0, (i, j) \in \mathcal{E}. \quad (21)$$

where  $\mathbf{z}_i(t) = [\mathbf{x}_i(t)^T, \mathbf{u}_i(t)^T]^T$  aggregates the states and inputs at time  $t$ .

This convexification based on linearization introduces some suboptimality but makes the problem tractable. The accuracy can be improved by linearizing updated trajectories iteratively.

## C. Problem Decomposition

To decompose the centralized optimization problem into tractable subproblems for each CAV, we introduce local copies of the coupling variables and consensus constraints [32] to equalize

the copies:

$$\min_{\mathbf{z}_i, \mathbf{z}_i^j, \forall j \in \mathcal{N}_i} \sum_i i = 1^N l_{\phi_i}(\mathbf{z}_i). \quad (22)$$

where  $\mathbf{z}_i^j$  is the copy of  $\mathbf{z}_i$  kept by vehicle  $i$ . The consensus constraints  $\mathbf{z}_i(t) = \mathbf{z}_i^j(t)$  ensure all copies are equal.

We can now decompose this problem into  $N$  subproblems, one for each CAV  $i$ :

$$\min_{\mathbf{z}_i, \mathbf{z}_i^j, \forall j \in \mathcal{N}_i} \sum_i i = l_{\phi_i}(\mathbf{z}_i). \quad (23)$$

These subproblems can now be solved in a parallel and distributed manner by the CAV agents.

### III. COOPERATIVE CONTROL OF CAV

#### A. Proposed Synchronous and Asynchronous ADMM Algorithms

We present an algorithm based on the ADMM to solve the decomposed problem in a synchronous and parallel fashion.

The augmented Lagrangian [33] for the consensus optimization problem are:

$$L(\mathbf{z}, \mathbf{z}^j, \boldsymbol{\lambda}) = l_{\phi_i}(\mathbf{z}_i) + \sum_{(i,j) \in \mathcal{E}}. \quad (24)$$

$$\boldsymbol{\lambda}_{ij}^T (\mathbf{z}_i - \mathbf{z}_j^i) + \frac{\rho}{2} \sum_{(i,j) \in \mathcal{E}} |\mathbf{z}_i - \mathbf{z}_j^i|^2. \quad (25)$$

where  $\boldsymbol{\lambda}_{ij}$  is the Lagrange multipliers for the consensus constraints and  $\rho$  is a penalty parameter.

The synchronous ADMM (sADMM) algorithm consists of the following update steps at each iteration  $k$ :

*Step 1:* Update  $\mathbf{z}_i$  by solving the subproblem for each CAV  $i$ :

$$\mathbf{z}_i^{k+1} \arg \min_{\mathbf{z}_i} \left( l_{\phi_i}(\mathbf{z}_i) + \frac{\rho}{2} \sum_{j \in \mathcal{N}_i} |\mathbf{z}_i - \mathbf{z}_j^{i,k} + \boldsymbol{\lambda}_{ij}^k|^2 \right). \quad (26)$$

*Step 2:* Update dual variables  $\boldsymbol{\lambda}_{ij}$ :

$$\boldsymbol{\lambda}_{ij}^{k+1} = \boldsymbol{\lambda}_{ij}^k + \rho \left( \mathbf{z}_i^{k+1} - \mathbf{z}_j^{i,k+1} \right). \quad (27)$$

*Step 3:* Update shared variables  $\mathbf{z}_j^i$ :

$$\mathbf{z}_j^{i,k+1} = \mathbf{z}_j^{k+1}, \forall j \in \mathcal{N}_i. \quad (28)$$

These steps are repeated until convergence. The  $\mathbf{z}_i$  updates can be performed independently in parallel by each CAV. After each iteration, the updated  $\mathbf{z}_i$  values are shared with neighbors.

We provide a brief convergence analysis for the sADMM algorithm.

Let  $\mathbf{z}$ ,  $\mathbf{z}_j$ , and  $\boldsymbol{\lambda}^*$  denote the optimal primal and dual variables. The primal residual at the  $k$ th iteration is:

$$\mathbf{r}^k = [\mathbf{z}^{k+1} - \mathbf{z}^{k+1,j}], (i,j) \in \mathcal{E}. \quad (29)$$

And the dual residual is:

$$\mathbf{s}^k = \rho [\mathbf{z}^{k+1,j} - \mathbf{z}^{k,j}], (i,j) \in \mathcal{E}. \quad (30)$$

The sADMM algorithm drives the primal and dual residuals to zero, i.e.,

$$\lim_{k \rightarrow \infty} \left| \mathbf{r}^k \right| = \lim_{k \rightarrow \infty} \left| \mathbf{s}^k \right| = 0. \quad (31)$$

To model the asynchrony, we track local iteration counts  $k_i$  for each CAV  $i$ . The update steps now become:

*Step 1:* Update  $\mathbf{z}_i$  by solving:

$$\mathbf{z}_i^{k_i+1} \arg \min_{\mathbf{z}_i} \left( l_{\phi_i}(\mathbf{z}_i) + \frac{\rho}{2} \sum_{j \in \mathcal{N}_i} |\mathbf{z}_i - \hat{\mathbf{z}}_j^{i,k_i} + \hat{\boldsymbol{\lambda}}_{ij}^{k_i}|^2 \right). \quad (32)$$

*Step 2:* Update dual variables  $\boldsymbol{\lambda}_{ij}$ :

$$\hat{\boldsymbol{\lambda}}_{ij}^{k_i+1} = \hat{\boldsymbol{\lambda}}_{ij}^{k_i} + \rho \left( \mathbf{z}_i^{k_i+1} - \hat{\mathbf{z}}_j^{i,k_i+1} \right). \quad (33)$$

*Step 3:* Broadcast  $\mathbf{z}_i$  to neighbors:

$$\hat{\mathbf{z}}_j^{k_i+1} = \mathbf{z}_i^{k_i+1}, \forall j \in \mathcal{N}_i. \quad (34)$$

The key difference is the use of delayed neighbor variables  $\hat{\mathbf{z}}_j$  and  $\hat{\boldsymbol{\lambda}}_{ij}$  since perfect synchronization is not guaranteed. Staleness of information degrades optimality but convergence can still be guaranteed under mild assumptions as shown next.

Assuming the delay is uniformly bounded by a finite constant  $\tau$ , and each CAV updates at least once within any  $B$  consecutive iterations. Under these assumptions, we can show the following convergence guarantee that the asynchronous ADMM (aADMM) algorithm converges to a neighborhood of the optimal solution, with neighborhood size proportional to the delay bound  $\tau$ .

For the sADMM algorithm, under the mild assumptions that the local subproblems solved by each CAV vehicle are convex and the unaugmented Lagrangian has a saddle point, the following convergence result holds:

$$\lim_{k \rightarrow \infty} \left| \mathbf{r}^k \right| = \lim_{k \rightarrow \infty} \left| \mathbf{s}^k \right| = 0. \quad (35)$$

This means primal and dual residuals converge to zero as the synchronous ADMM iterations progress. Therefore, convergence to the optimal centralized trajectory coordination solution is guaranteed. A similar result is shown for the asynchronous ADMM case under additional assumptions bounding the delay and ensuring all vehicles update periodically. This convergence guarantee proves the distributed algorithm's ability to coordinate the CAV platoon optimally.

#### B. Distributed Training Scheme

LMs powered by deep learning have emerged as a powerful tool for modeling complex transportation systems with many interacting components. Here, we propose a distributed training scheme where each CAV trains its cost and dynamics networks on simulators local to each vehicle. A central coordinator interacts with the vehicles to tune the coupling networks.

In this method, we consider a CAV fleet with  $n$  vehicles labeled  $1, \dots, n$ . Each CAV  $i$  has a local simulator that can generate training data for learning the vehicle's cost network  $f_i(x_i)$  and dynamics network  $g_i(x_i, u_i)$ . The goal is to train these networks in a distributed manner while coordinating between vehicles.

The overall workflow contains three main steps:

*Step 1:* Local model training

In the first step, each CAV trains its cost and dynamics networks on data generated from its local simulator.

The local loss function to be minimized is:

$$\mathcal{L}_i(\theta_{f_i}, \theta_{g_i}) = \frac{1}{N_i} \sum_{k=1}^{N_i} l(f_i(x_i^k; \theta_{f_i}), y_{f_i}^k) + l(g_i(x_i^k, u_i^k; \theta_{g_i}), y_{g_i}^k). \quad (36)$$

where  $x_i^k$ ,  $u_i^k$ ,  $y_{f_i}^k$ , and  $y_{g_i}^k$  are state, control input, cost target, and next state samples for vehicle  $i$ .  $f_i$  and  $g_i$  represent the cost and dynamics networks parameterized by  $(\theta_{f_i}, \theta_{g_i})$ .  $l(\cdot)$  is the loss function.  $N_i$  is the number of samples from vehicle  $i$ 's simulator.

This trains models customized for each vehicle using local data. The trained networks are used as initialization for the next step.

*Step 2: ADMM for coupled training*

In the second step, we want to coordinate the vehicle models by introducing coupling terms in the cost functions:

$$f_i(x_i) + c_{ij}(x_i, x_j), \forall j \in \mathcal{N}_i. \quad (37)$$

where  $\mathcal{N}_i$  is the set of neighboring vehicles of  $i$ , and  $c_{ij}(\cdot)$  couples  $i$  and  $j$ 's states.

To learn the coupling terms in a decentralized way, we formulate the following optimization problem with consensus constraints:

$$\min_{c_{ij}} \sum_{i=1}^n \left[ L_i(f_i + c_{ij}) + \frac{\lambda}{2} |c_{ij}|^2 \right] \quad \text{s.t. } c_{ij} = c_{ji}, \forall j \in \mathcal{N}_i. \quad (38)$$

where  $L_i(\cdot)$  is the loss function for CAV  $i$  combining cost and dynamics.

This can be solved using the ADMM approach similar to the classification case. The update steps are:

$$\begin{cases} c_{ij}^{k+1} = \arg \min_{c_{ij}} L_i(f_i + c_{ij}) + \frac{\rho}{2} |c_{ij} - u_{ij}^k|^2 \\ c_{ji}^{k+1} = \arg \min_{c_{ji}} L_j(f_j + c_{ji}) + \frac{\rho}{2} |c_{ji} - u_{ji}^k|^2 \\ \bar{c}_{ij}^{k+1} = \frac{1}{2} (c_{ij}^{k+1} + c_{ji}^{k+1}) \\ u_{ij}^{k+1} = u_{ij}^k + c_{ij}^{k+1} - \bar{c}_{ij}^{k+1} \\ u_{ji}^{k+1} = u_{ji}^k + c_{ji}^{k+1} - \bar{c}_{ji}^{k+1} \end{cases}. \quad (39)$$

where  $\bar{c}_{ij}$  is the averaged coupling term,  $\rho$  is the penalty, and  $u_{ij}$  is the dual variable. The  $c_{ij}$  updates can be done in parallel per edge. After convergence, we obtain consensus couplings  $\bar{c}_{ij}$ .

*Step 3: Local model update*

Finally, each CAV updates its cost network using the consensus coupling terms:

$$\tilde{f}_i(x_i) = f_i(x_i) + \sum_{j \in \mathcal{N}_i} \bar{c}_{ij}(x_i, x_j). \quad (40)$$

The local cost networks are retrained to minimize loss on the updated cost function:

$$\min_{\theta_{f_i}} \frac{1}{N_i} \sum_{k=1}^{N_i} l(\tilde{f}_i(x_i^k; \theta_{f_i}), y_{f_i}^k). \quad (41)$$

The dynamics networks  $g_i(\cdot)$  can also be fine-tuned if needed. This yields cost and dynamics models customized for each CAV but coordinated through the coupling terms.

*C. Car-Following Model and Strategy for Mixed-Traffic Flow*

The car-following model is integral to the future of transportation and vehicle technology primarily because it underpins a wide range of critical developments [34], [35]. Car-following models are crucial in evaluating the environmental footprint of road traffic, including emissions and fuel consumption, thereby facilitating the development of more sustainable transportation policies [36], [37].

Subsequently, we propose a new car-following model called the integrated velocity and acceleration fusion (IVAF) model that integrates state information from multiple lead and following vehicles to determine the optimal acceleration for the subject CAV.

The proposed IVAF model builds on previous models, e.g., optimal velocity changes with memory and multiple vehicles changes memory, but incorporates additional terms to account for the accelerations of the immediate lead and following vehicles as well as exponentially smoothed velocity differences from multiple vehicles:

$$\begin{aligned} \ddot{x}_n(t) = & a [pV_F[\Delta x_n(t)] + (1-p)V_B[\Delta x_{n-1}(t)] - \dot{x}_n(t)] \\ & + \lambda_1 E(n, k) + \lambda_2 E(n, h) + \omega_1 \ddot{x}_{n+1}(t) + \omega_2 \ddot{x}_{n-1}(t) \\ & + \sum_{i=1}^k \gamma_i V_F[\Delta x_{n+i-1}(t)] \\ & - V_F[\Delta x_{n+i-1}(t - \tau)] \\ & + \sum_{j=1}^h \gamma_j V_B[\Delta x_{n-j}(t)] - V_B[\Delta x_{n-j}(t - \tau)]. \end{aligned} \quad (42)$$

where  $V_F$  and  $V_B$  are optimal velocity functions for lead and following vehicles.  $E(n, k)$  and  $E(n, h)$  are exponentially smoothed velocity differences from  $k$  lead and  $h$  following vehicles.  $\omega_1, \omega_2$  are sensitivities to immediate lead and following vehicle accelerations.  $\gamma_i, \gamma_j$  account for velocity trend memory effects.

$$\begin{cases} V_F[\Delta x_n(t)] = \alpha_1 \tanh[\Delta x_n(t) - h_s] + \tanh(h_s) \\ V_B[\Delta x_n(t)] = -\alpha_2 \tanh[\Delta x_n(t) - h_s] + \tanh(h_s) \end{cases}. \quad (43)$$

$$\begin{cases} E(n, k) = \beta \sum_{j=0}^{k-2} (1-\beta)^j \Delta v_{n+j+1}(t) \\ E(n, h) = \beta \sum_{l=0}^{h-1} (1-\beta)^l \Delta v_{n-l-1}(t) \end{cases}. \quad (44)$$

Let  $\mathbf{x} = [\Delta x_n, \Delta v_n]^T$ . The linearized model around the equilibrium point  $\mathbf{x}^*$  is:

$$\dot{\mathbf{x}} = \mathbf{A} \mathbf{x}. \quad (45)$$

where  $\mathbf{A}$  is a  $2 \times 2$  matrix containing linearized dynamics parameters that characterize the stability of the proposed car-following

model.

$$\mathbf{A} = \begin{bmatrix} 0 & 1 \\ a[pV'_F(b) - (1-p)V'_B(b)] & 1^h \gamma_j z_1 \end{bmatrix}. \quad (46)$$

The eigenvalue of  $\mathbf{A}$  is:

$$\lambda = \frac{-tr(\mathbf{A}) \pm \sqrt{tr^2(\mathbf{A}) - 4det(\mathbf{A})}}{2}. \quad (47)$$

It can be shown that for suitable parameter choices, the real part of  $\lambda$  is negative, indicating local stability around the equilibrium point.

String stability indicates attenuation of disturbances along a string of vehicles. To analyze this, we study how perturbations propagate through the vehicle string by substituting  $\Delta x_n(t) = Ae^{\phi n + zt}$  into the linearized IVAF model:

$$\begin{aligned} z^2 &= a[pV'_F(b)(e^\phi - 1) - (1-p)V'_B(b)(e^{-\phi} - 1) - z] \\ &+ \lambda_1 \beta k z \sum_{j=0}^{k-2} (1-\beta)^j e^{\phi(j+1)} \\ &+ \lambda_2 \beta h z \sum_{l=0}^{h-1} (1-\beta)^l e^{-\phi(l+1)} + z^2(w_1 + w_2)e^\phi \\ &+ \tau V'_F(b) \sum_{i=1}^k \gamma_i [e^{\phi i} - e^{\phi(i-1)}] \\ &+ \tau V'_B(b) \sum_{j=1}^h \gamma_j [e^{-\phi j} - e^{-\phi(j-1)}]. \end{aligned} \quad (48)$$

The characteristic equation yields:

$$\begin{aligned} z_2 &= \frac{1}{2} [pV'_F(b) - (1-p)V'_B(b)] + \frac{1}{a} \left[ \lambda'_1 \sum_{j=0}^{k-2} (1-\beta)^j z_1 \right. \\ &+ \lambda'_2 \sum_{l=0}^{h-1} (1-\beta)^l z_1 + (w_1 + w_2 - 1) z_1^2 \\ &\left. + \tau V'_F(b) \sum_{i=1}^k \gamma_i z_1 + \tau V'_B(b) \sum_{j=1}^h \gamma_j z_1 \right]. \end{aligned} \quad (49)$$

where  $z_1 = pV'_F(b) + (1-p)V'_B(b)$  and  $z_2$  is the second characteristic root governing string stability. The stability condition is:

This provides theoretical guidance on selecting parameters like  $a$ ,  $k$ , and  $h$  to ensure string stability of the IVAF model.

Comparatively, CAVs leverage advanced wireless communication to continuously acquire extensive motion data about the vehicle and the road. This capability facilitates autonomous environmental perception, decision-making, and control processes in CAVs, significantly enhancing their ability to preempt

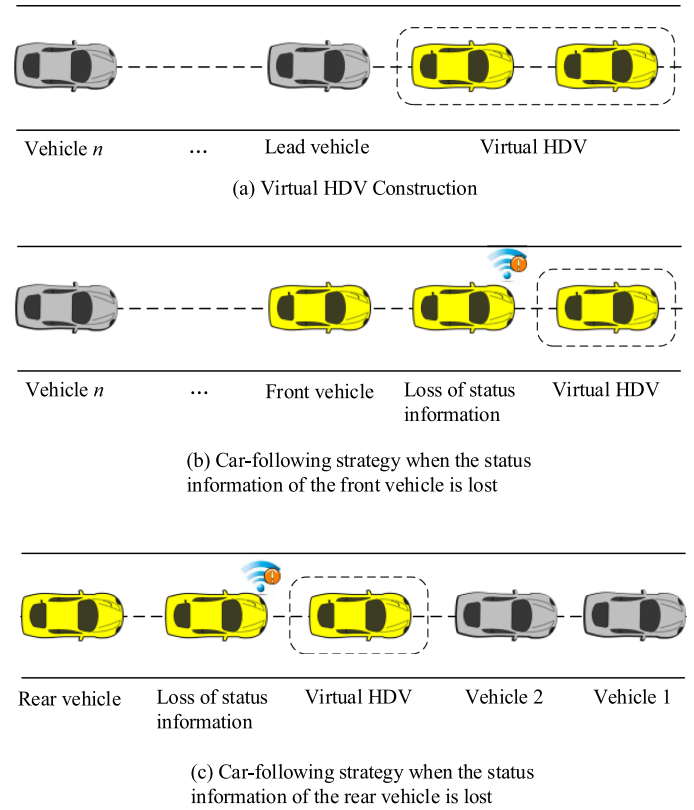


Fig. 1. Car-following strategy.

and prevent traffic incidents. The dichotomy in the operational dynamics of HDVs and CAVs within a mixed traffic environment is exemplified in the car-following strategy, depicted in Fig. 1.

Combining the findings and methodologies with driver behavior model-based simulation calibration, we aim to enhance the calibration process of our driver behavior models [38], [39]. We employ real-world data to tune model parameters, utilize optimization techniques to minimize discrepancies between simulated and observed behaviors and validate our models using diverse datasets, which will ensure that our models accurately capture the complexities of driver behavior in mixed traffic scenarios, improving the overall realism and reliability of our study.

After applying the distributed optimal control strategy, the vehicle platoon reaches an optimized formation that maximizes traffic flow and safety. However, this platoon must still demonstrate resilience against real-world uncertainties like sudden braking by the lead vehicle. To guarantee string stability, mathematically derive the condition on the control gain parameter  $a$  to ensure any disturbances introduced on the lead CAV will decay as it propagates to the subsequent vehicles.

Essentially, (50) shown at the bottom of this page, provides a lower bound threshold for the control gain  $a$ . As long as the CAV vehicles tune their control gains to satisfy this threshold,

$$a > \frac{-2 \left[ \lambda'_1 z_1 + \lambda'_2 z_1 + (w_1 + w_2 - 1) z_1^2 + \tau V'_F(b) \sum_{i=1}^k \gamma_i z_1 + \tau V'_B(b) \right]}{[pV'_F(b) - (1-p)V'_B(b)]}. \quad (50)$$

the optimized platoon can attenuate any disturbances - proving resilience against real-world uncertainties. This mathematical derivation of the string stability condition supplies a formal guarantee that the distributed multi-vehicle coordination algorithm yields an optimized CAV platoon that is provably stable against upstream propagations.

#### D. Graph Neural Network-based Vehicle Driving Intention Recognition and Trajectory Prediction

In actual driving scenarios, at time  $t$  at position  $i$ , there may be no surrounding vehicles for the one being predicted. In this case, it can be assumed that at time  $t$  for position  $i$ , the distance to the predicted vehicle is infinitely large, and the vehicle state parameters at position  $i$  at time  $t$  can be set to  $S_i^{(t)} = [10000, 10000, 0, 0, 0, 0]$ .

This subsection utilizes graph sample and aggregate -based neural network and the GRU (GSAG-GRU), proposing a model for recognizing driving intentions and predicting the trajectories of surrounding vehicles based on these theories [40].

The ability to model complex interactive relationships between entities is central to accurately recognizing driving intentions. Graph neural networks are designed to capture such relational reasoning by operating on graph-structured data representing vehicle pairwise interactions. In contrast, CNNs focus more on extracting spatial features from sensor inputs but cannot sufficiently encode semantic connections between vehicles that provide critical contextual cues for intention recognition. Likewise, Transformers specialize in sequential modeling and long-range dependencies in time. However, the self-attention mechanism lacks an explicit relation-centric inductive bias. Transformers need help fully incorporating the navigational dependencies essential for multi-agent driving scenarios.

On the other hand, GRUs balance model performance and computational requirements for online trajectory forecasting. LSTMs can achieve slightly higher accuracy but involve more parameters and processing. Transformer architectures incur even higher complexity costs. Considering the need to deploy intention recognition and motion prediction models on autonomous vehicles with power and latency constraints, GRUs offer an optimal fit.

While graph neural networks and gated recurrent units have become ubiquitous for relational and sequential modeling, respectively, this study incorporates specialized enhancements to cater their architectures to the distinct complexities and challenges of forecasting vehicle trajectories in dynamic traffic environments. Specifically, we use the GraphSAGE network as the foundation for capturing the spatial and temporal interactions among vehicles in the traffic environment. The GraphSAGE network allows for efficient aggregation of neighborhood information and enables learning meaningful representations for each vehicle node in the graph. To further enhance the expressiveness and adaptability of our model, we introduce multi-edge convolutions and spatiotemporal connectivity modeling within the GraphSAGE framework. The multi-edge convolutions enable the network to capture diverse vehicle interactions and

relationships, such as relative positions, velocities, and accelerations. We can model complex dynamics and dependencies in real-world traffic scenarios by incorporating multiple edge types. Furthermore, we extend the GraphSAGE network with spatiotemporal connectivity modeling, which allows for the propagation of information across neighboring vehicles and different time steps. This enhancement enables the network to capture the evolution of vehicle states and interactions over time, providing a more comprehensive understanding of the traffic flow. These specialized enhancements are seamlessly integrated into the GraphSAGE network structure, enabling our model to effectively capture the intricate spatial and temporal patterns in traffic data. Combining multi-edge convolutions, spatiotemporal connectivity modeling, and the GraphSAGE network architecture results in a powerful and flexible framework for vehicle trajectory prediction and interaction modeling.

The proposed methodology is beneficial to CACC vehicles and flow modeling and control. First, it introduces a novel IVAF model that incorporates state information from multiple leads and following vehicles to determine optimal acceleration for the subject CAV and enhances situational awareness and cooperative capabilities compared to traditional CACC models. Second, this study uses graph neural networks and gated recurrent units to recognize driving intentions and predict trajectories of surrounding vehicles, enabling more accurate modeling of complex vehicle interactions in mixed traffic scenarios. Third, the distributed optimization framework using synchronous and asynchronous ADMM algorithms allows for efficient coordination of large-scale CAV fleets, addressing scalability challenges often encountered in previous studies. Furthermore, the proposed methodology is validated through extensive simulations, demonstrating improved traffic efficiency, safety, and robustness under various scenarios. By integrating advanced machine learning techniques, distributed optimization, and enhanced car-following models, this study pushes the boundaries of existing traffic flow management approaches for CACC vehicles [41], [42]. It provides a comprehensive framework for modeling, controlling, and coordinating CAVs in mixed-traffic environments, contributing to developing more intelligent and efficient transportation systems.

Additionally, the increased presence of CACC vehicles led to a notable reduction in emissions, as the optimized traffic flow minimized stop-and-go behavior and excessive accelerations [43], [44]. The emission levels decreased proportionally with the increase in CACC penetration, highlighting the environmental benefits of the proposed strategies [45]. Further, safety metrics, such as time-to-collision and the number of critical events, exhibited substantial improvements as the CACC penetration rate increased. The collaborative nature of the CACC vehicles enabled better anticipation and response to potential conflicts, thereby enhancing overall traffic safety [46]. These demonstrate the effectiveness and scalability of the proposed CACC control strategies in improving network-wide performance across multiple dimensions, emphasizing their potential for real-world implementation in mixed-traffic environments.

Overall, the diagram of cooperative control of CAV is shown in Fig. 2.

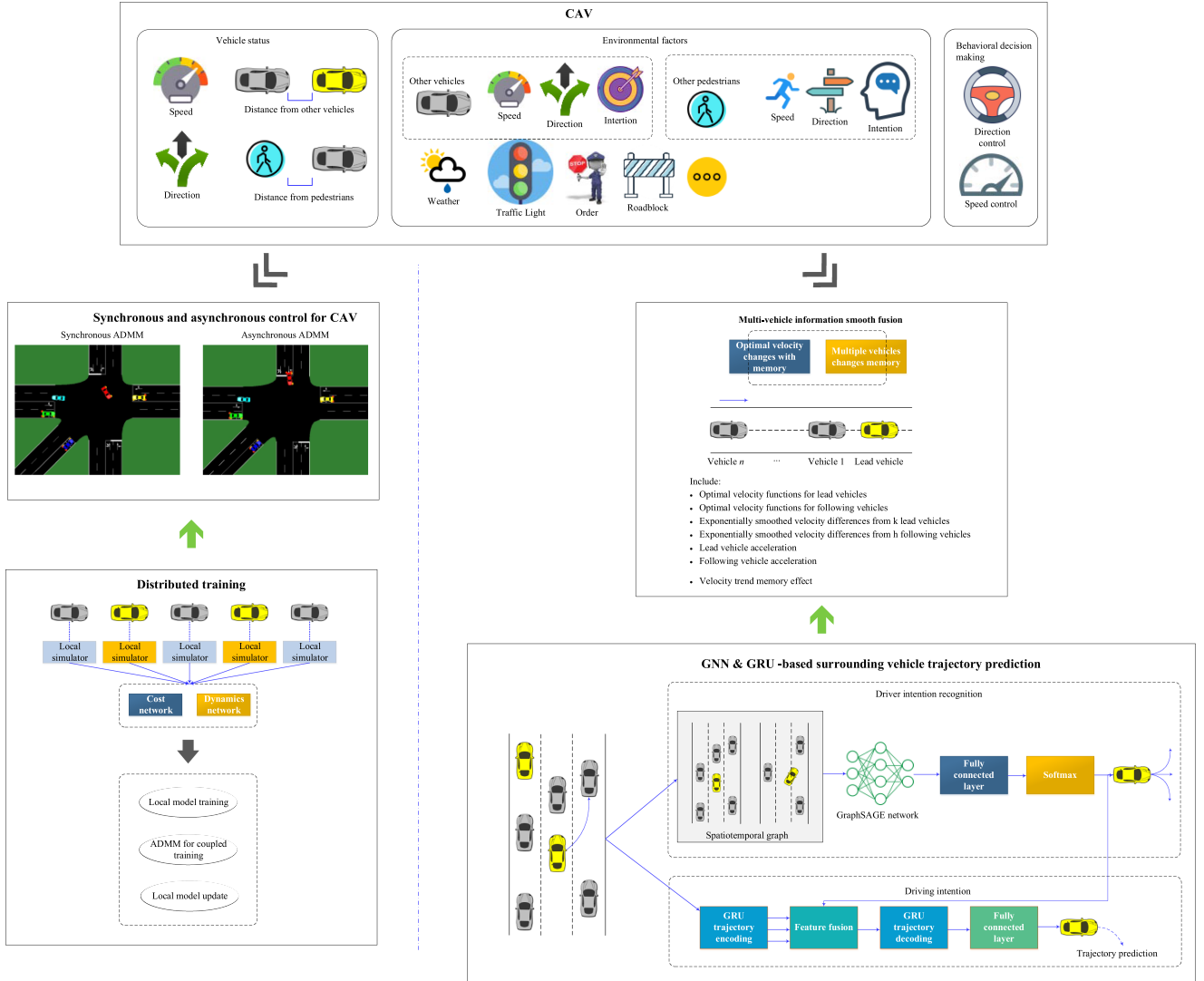


Fig. 2. Diagram of cooperative control of CAV.

#### IV. SIMULATION AND RESULTS ANALYSIS

##### A. Performance Evaluation of Synchronous and Asynchronous ADMM

We present numerical simulations to demonstrate the proposed algorithms. The CAV dynamics are modeled by the discrete-time unicycle model [47]:

$$\begin{cases} x_{i,k+1} = x_{i,k} + v_i \Delta t \cos(\theta_{i,k}) \\ y_{i,k+1} = y_{i,k} + v_i \Delta t \sin(\theta_{i,k}) \\ \theta_{i,k+1} = \theta_{i,k} + \omega_i \Delta t \end{cases} \quad (51)$$

where  $(x_i, y_i)$  is the position,  $\theta_i$  is the heading angle,  $v_i$  is the constant speed,  $\omega_i$  is the turn rate, and  $\Delta t$  is the sampling time. The control input is  $u_i = \omega_i$ .

The cost function penalizes deviation from a straight line reference path:

$$l_{\phi_i}(x_i, y_i) = (x_i - x_i^{ref})^2 + (y_i - y_i^{ref})^2. \quad (52)$$

The coupling cost penalizes proximity between vehicles:

$$c_{\psi_{ij}}(x_i, x_j, y_i, y_j) = \frac{1}{|p_i - p_j|^2}. \quad (53)$$

where  $p_i = (x_i, y_i)$  and  $p_j = (x_j, y_j)$  are the positions.

The collision avoidance constraints are linearized as:

$$(x_i - x_j)^2 + (y_i - y_j)^2 \geq d_{safe}^2 \approx \mathbf{H}_{ij} z_i + \mathbf{J}_{ij} z_j \geq 0. \quad (54)$$

where  $z_i = (x_i, y_i, \theta_i, \omega_i)$  aggregates the states and input.

We simulate a fleet of  $N = 5$  CAVs moving through an intersection, starting from random initial positions. The horizon length is  $T = 10$ . Algorithm parameters are  $\rho = 1$ ,  $\epsilon_{abs} = 10^{-5}$ ,  $\epsilon_{rel} = 10^{-3}$ . The delay bound for the asynchronous algorithm is  $\tau = 5$ .

The effectiveness of the proposed sADMM and aADMM algorithms as cooperative control strategies are validated through simulation experiments. We examine and analyze the results before and after optimal control is applied to facilitate comparative analysis. The scenario involves a four-way intersection with



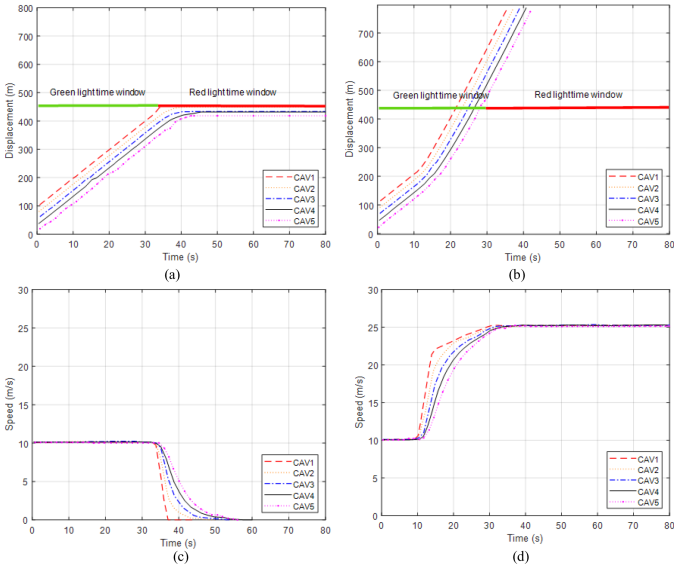


Fig. 3. Simulation results in scenario 1.

traffic lights, where the north-south and east-west directions each consist of 2-lane roads, including a left turn lane. The dimensions of the intersection are 50 meters by 50 meters.

In the first scenario, denoted as scenario 1, the traffic signal initially displays the green phase, with a time window of  $[0, 30 \text{ s}]$ . The simulation outcomes, depicted in Fig. 3, reveal that at the outset, the fleet of vehicles travels at a speed of 10 meters per second. Without optimized control, the CAVs continue constantly and fail to utilize the initial green phase (time window:  $[0, 30 \text{ s}]$ ). Consequently, they arrive at the stop line during the red phase, necessitating a complete stop and waiting for the subsequent green phase.

In scenario 2, assuming that the signal is in the red phase at the initial moment, the first green time window is  $[40, 70 \text{ s}]$ , and other initial conditions are the same as in scenario 1; the simulation results are shown in Fig. 4.

As depicted in Fig. 4, the CAV fleet maintains a constant speed under uncontrolled conditions. The traffic signal is in the red phase when it approaches the stop line. The signal switches to the green phase following a brief stop-and-wait period. At this point, the CAV vehicles gradually accelerate and proceed past the stop line. Upon implementing aADMM, the lead vehicle of the CAVs undergoes a speed adjustment process characterized by minimal amplitude changes. This adjustment ensures that all CAV vehicles successfully traverse the intersection within the green light time window without necessitating stops. Consequently, this optimization enhances passenger comfort significantly and facilitates uninterrupted passage.

The application of large models, particularly the sADMM and aADMM algorithms, in the cooperative control of CAVs demonstrates substantial benefits in optimizing vehicular traffic flow, enhancing safety, and improving ride comfort. By integrating these algorithms, CAVs can effectively utilize traffic light phases, reducing unnecessary stops and delays.

In scenarios where vehicles must traverse intersections with traffic signals, the sADMM algorithm enables the lead vehicle

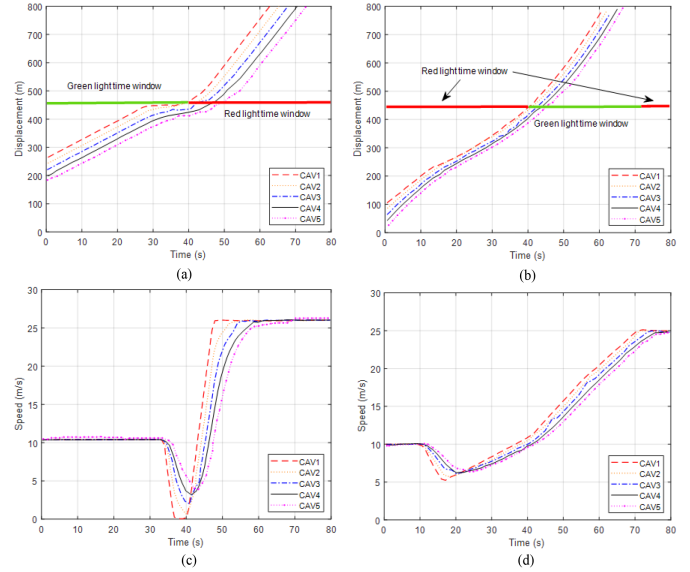


Fig. 4. Simulation results in scenario 2.

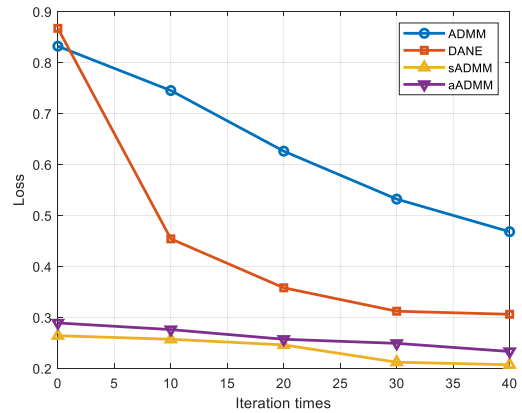


Fig. 5. Convergence comparison.

to optimize its trajectory by considering its performance and the overall fleet’s efficiency. This results in smoother and more efficient traffic flow, as the vehicles can accelerate or decelerate appropriately to pass through the intersection during the green phase, thus avoiding stops at red lights. Such optimization significantly reduces fuel consumption and minimizes the stop-and-go behavior commonly associated with traffic light-controlled intersections.

The convergence plots in Fig. 5 show that the sADMM algorithm achieves lower residuals faster while the aADMM algorithm also converges.

Table I shows the Computation Time, Speedup over ADMM, and Fleet scalability to demonstrate the proposed distributed coordination algorithms’ efficiency. While computation time is measured in milliseconds of wall-clock time taken per optimization step. Speedup over ADMM compares runtime improvement over the benchmark decentralized method. Fleet scalability evaluates the increase in computation time as the number of vehicles grows from 10 CAVs to 100 CAVs.

TABLE I  
COMPARISON OF COMPUTATIONAL LOAD AND ROBUSTNESS

Fleet size	Computation time (ms)	Speedup over ADMM	Fleet scalability
ADMM	28	1X	4.1X
DANE	23	1.2X	3.8X
sADMM	18	1.6X	1.3X
aADMM	16	1.8X	1.1X

TABLE II  
COMPARISON OF CAR-FOLLOWING MODELS

Metric	IDM	W99	CACC	IVAF
String stability	0.85	0.79	0.87	0.93
Disturbance attenuation	4.26 m/s <sup>2</sup>	3.81 m/s <sup>2</sup>	3.99 m/s <sup>2</sup>	2.74 m/s <sup>2</sup>
Velocity Fluctuation	3.45 m/s	3.16 m/s	3.32 m/s	2.28 m/s

The results showcase the proposed sADMM and aADMM algorithms have significantly lower computation time that scales more evenly with increasing vehicles compared to ADMM or DANE.

Activation of the sADMM algorithm enables the lead CAV to optimize its velocity by factoring in the current green phase duration as well as the overall fleet efficiency. By appropriate acceleration, the lead CAV can ensure that all five CAVs traverse the intersection without stopping during the first green phase. utilizing traffic light information for cooperative control eliminates wasteful deceleration, idling, and acceleration, enhancing transportation efficiency, reducing fuel usage and emission, and improving ride comfort by preventing stops.

The integration of large models using the sADMM and aADMM algorithms in the control of CAVs highlights several positive impacts crucial for advancing intelligent transportation systems. Additionally, a standout feature of both the sADMM and aADMM algorithms is their consistent computation time, which remains nearly constant regardless of the fleet size.

### B. Performance Comparison With Different Vehicle Parameters

To verify the effectiveness of the CAV following model and optimization strategy in the mixed traffic environment, this paper assumes that all vehicles on the road follow the following driving mode, i.e., only longitudinal behavior is considered, no consideration of lateral behavior, no lane changing, pedestrians, non-motorized vehicles and other traffic factors interfere, and the braking stop and start two scenarios can intuitively reflect the following behavior of the vehicle. Therefore, in this subsection, three simulation scenarios of vehicle braking and stopping, starting, and running without boundary conditions are selected in the mixed traffic environment, among which the braking, stopping, and starting scenarios are mainly designed for verifying the multi-vehicle state information cognition and key information fusion.

We simulate the scenario of the IVAF follow-along model when the fleet vehicles start as follows: during the start-up

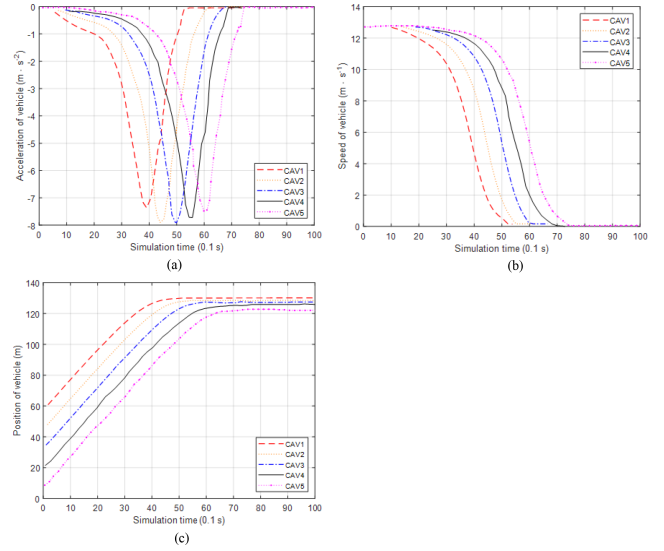


Fig. 6. Changes in vehicle parameters during braking and deceleration.

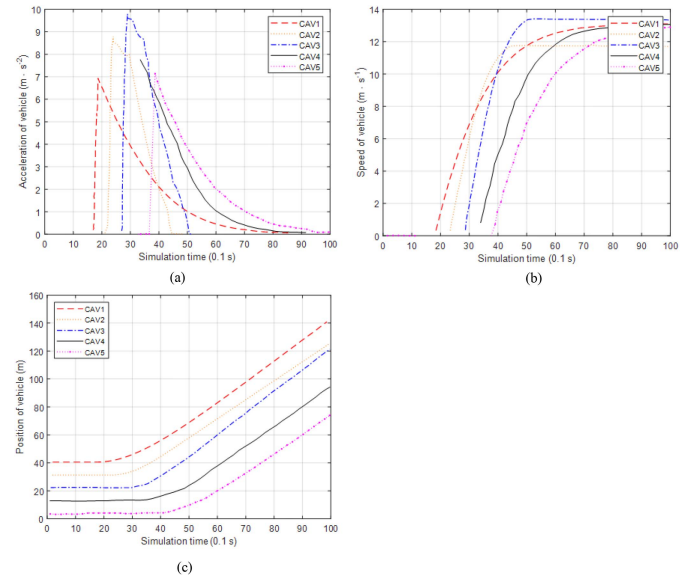


Fig. 7. Changes in vehicle parameters during acceleration.

process, the initial speed of the ten vehicles are all 0, and all of them are at a standstill, and the position of each vehicle is  $x_n(0) = (n - 1)\Delta x_n(t)$ , and when  $t = 0$ , the lead vehicle accelerates to 3 m/s<sup>2</sup> for a start and keeps this speed at a uniform speed when it accelerates to 12.8 m/s<sup>-1</sup>. After the lead vehicle accelerates, the other nine vehicles in the fleet follow one by one. The results are shown in Fig. 6.

The acceleration, velocity, position, and headway of vehicles 1 to 5 are selected for the study. As can be seen in Fig. 7, the acceleration changes of vehicles 2 and 3 are more significant, and vehicle 4, because of following the CAV, has a peak difference of 1 m/s<sup>-2</sup> relative to vehicle 1, so that the acceleration performance of vehicle 5 is also better than that of vehicle 1. Therefore, the speed changes of vehicles 2 and 3 are faster relative to the other vehicles.

TABLE III  
COMPARISON OF DRIVING INTENTION RECOGNITION

Models	Driving intentions	Number of samples	Number of correct identifications	Accuracy	Mean accuracy
GSAG-GRU	Left lane change	1698	1576	92.81%	94.60%
	Straight-line driving	1698	1579	92.99%	
	Right lane change	1698	1664	98.00%	
Hiformer	Left lane change	1698	1523	89.69%	92.83%
	Straight-line driving	1698	1538	90.58%	
	Right lane change	1698	1668	98.23%	
T-transformer	Left lane change	1698	1547	91.11%	92.27%
	Straight-line driving	1698	1533	90.28%	
	Right lane change	1698	1620	95.41%	
LAS-Transformer	Left lane change	1698	1542	90.81%	93.89%
	Straight-line driving	1698	1573	92.64%	
	Right lane change	1698	1668	98.23%	
R-Transformer_BiLSTM	Left lane change	1698	1577	92.88%	92.25%
	Straight-line driving	1698	1523	89.69%	
	Right lane change	1698	1599	94.17%	
HT-Net	Left lane change	1698	1498	88.22%	92.83%
	Straight-line driving	1698	1570	92.46%	
	Right lane change	1698	1661	97.82%	
GCN	Left lane change	1698	1489	87.69%	84.84%
	Straight-line driving	1698	1236	72.79%	
	Right lane change	1698	1597	94.05%	
LSTM	Left lane change	1698	1515	89.22%	86.57%
	Straight-line driving	1698	1238	72.91%	
	Right lane change	1698	1657	97.59%	

To summarize, when the lead vehicle of the fleet driving at a uniform speed in the mixed traffic environment receives the disturbance signal, the higher the CAV penetration rate of the fleet using the IVAF car-following model and car-following strategy, the shorter the overall recovery time to the stationary state, and the less severe the disturbance.

The application of large models, specifically the IVAF follow-along model, in CAVs within a mixed-traffic environment has shown promising results in enhancing traffic flow dynamics and overall vehicular performance. The effectiveness of this model is evident in scenarios involving braking, acceleration, and maintaining steady speeds, where it significantly improves the response and coordination among CAVs.

Subsequently, we demonstrate the advantages of the proposed IVAF model over three established car-following models: intelligent driver model (IDM), Wiedemann 99 (W99) [48], and cooperative adaptive cruise control (CACC) [49]. The metrics used for evaluation are: (1) string stability, analyzing how disturbances propagate through a platoon of vehicles; (2) disturbance attenuation, measuring the impact of disturbances introduced to the lead vehicle on the velocity fluctuations of following vehicles; and (3) velocity fluctuation, comparing fluctuations in velocity profiles between models. The simulation setup is a

platoon of 10 vehicles traveling in a single lane. The lead vehicle introduces velocity disturbances by changing its acceleration. Table II shows a quantitative comparison between models.

The results demonstrate that IVAF has better string stability, lower disturbance impacts, and more minor velocity fluctuations compared to IDM, W99, and CACC models, validating the performance benefits of the proposed IVAF car-following model.

We construct an integrated autonomous driving dataset combining sequences from multiple public sources. The NGSIM US-101 and I-80 highway datasets are sourced from the Next Generation Simulation data made accessible by the US Federal Highway Administration, comprising overhead recordings of trajectory data across thousands of frames of highway traffic. This contains 20543 instances of left lane changes, 31747 instances of straight driving, and 8491 instances of right lane changes within dense traffic scenarios. The nuScenes dataset spanning Boston and Singapore, providing 1000 scenes (20 seconds each) with full vehicle trajectory annotations, offers geographical, environmental, and traffic density diversity across urban areas. The ApolloScape dataset compiles trajectories via tracking algorithms applied to extensive traffic video footage from Chinese cities and offers a cross-cultural evaluation of interaction behavior models. Any biases are mitigated through

a balanced sampling of data chunks for each labeled maneuver category. The datasets are partitioned: 80% for training (20590 sequences) and 20% for testing (5148 sequences).

To appraise the driving intention recognition model, we compile 1698 real-world highway events covering lane changes and straight-line driving for benchmarking. The reference coordinates for the predicted vehicle in each frame provide the point of perspective. The proposed GSAG-GRU for trajectory forecasting contains approximately 9.2 million parameters distributed across the encoder, decoder, and auxiliary projection heads. While this places the model in the small-medium scale range, it is still quite large for deployment on autonomous vehicle hardware with memory and latency constraints. Subsequently, we conducted a comparative analysis with four alternative recognition models: The graph convolution network (GCN) recognition model, the driving intention recognition model built upon long short-term memory networks (LSTMs), sequence modeling networks with hierarchical attention mechanisms (Hiformer) [50], cross-attention based two-branch transformer network for rotating bearing fault diagnosis (T-transformer) [51], enhanced transformer based on the local attention mechanism for speech recognition (LAS-Transformer) [52], R-Transformer\_BiLSTM model [53], and hierarchical context-attention transformer network for medical CT image segmentation (HT-Net) [54]. The outcomes of this comparative analysis, showcasing the recognition performance, are presented in Table III. Table III demonstrates a notable improvement in the recognition accuracy of the GSAG-GRU algorithm.

To evaluate the effectiveness of the trajectory prediction model within a 5-second prediction time domain, we select the root mean square error (RMSE), average displacement error (ADE), and final displacement error (FDE) as the chosen metric for evaluation.

$$\text{RMSE} = \sqrt{\frac{\sum_{i=1}^n (x_i - x'_i)^2 + (y_i - y'_i)^2}{n}}. \quad (55)$$

where  $n$  is the total number of predicted trajectory coordinates,  $x_i, y_i$  are the true values of transverse and longitudinal coordinates respectively, and  $x'_i, y'_i$  are the predicted values of transverse and longitudinal coordinates respectively.

The RMSE, ADE, and FDE results of each trajectory prediction model comparing multiple-attention encoding-decoding framework (MAED) [55], trajectory prediction considering the behavior of pedestrians intersecting with vehicles (PB-TP) [56], attention mechanism-based spatial, dynamic, temporal interaction (SDT-ATT) [57], social-attention LSTM (SA-LSTM) [58] model, and vehicle trajectory prediction method based on time-feature encoding and physics-intention decoding (TFE-PID) [59] without considering driving intention are shown in Table IV.

Table IV reveals that the trajectory prediction model developed in this study, incorporating driving intention, achieves the highest accuracy in predicting the forthcoming vehicle motion trajectory within both long and short-time domains.

Table V shows the traffic throughput, safety, and energy efficiency of the overall integrated system on traffic efficiency. Traffic throughput is measured as the number of vehicles passing

TABLE IV  
COMPARISON OF RMSE, ADE, AND FDE

	RMSE	ADE	FDE
MAED	0.742	0.630	1.168
PB-TP	0.738	0.622	1.105
SDT-ATT	0.692	0.589	1.264
SA-LSTM	0.667	0.601	1.012
TFE-PID	0.634	0.526	0.937
GSAG-GRU	0.530	0.439	0.857

TABLE V  
COMPARISON OF TRAFFIC EFFICIENCY

Scenario	Traffic throughput (vehicle/hour)	Safety (TTC - seconds)	Energy efficiency (kJ/vehicle-mile)
Low density	560	4.2	5.6
Low density with control*	720 (+28%*)	3.1 (-26%*)	3.2 (-43%*)
High density	410	8.7	9.8
High density with control*	680 (+66%*)	5.2 (-40%*)	4.1 (-58%*)

Note: \*Improvement over no control

through the intersection over the simulation period. The time-to-collision metric evaluates safety. Energy efficiency is estimated as the kinetic energy consumption over the simulation.

It can be observed from Table V that enhanced transportation metrics across throughput, safety, and efficiency dimensions when applying the proposed integrated control framework validate its ability to orchestrate CAV movements to improve overall traffic flow.

## V. CONCLUSION

In this paper, we proposed a novel and promising approach for advancing the integration of LMs into future vehicles and transportation systems. The proposed algorithms based on the ADMM offer a distributed optimization framework for CAV fleets' cooperative control and coordination. The synchronous and aADMM algorithms allow for parallelized coordination, addressing scalability challenges in large-scale CAV systems. Furthermore, a distributed training scheme was introduced, enabling each CAV to train its cost and dynamics networks locally on simulators. The central coordinator fine-tunes the coupling networks through interactions with the vehicles, contributing to the overall efficiency and adaptability of the system. Integrating a new car-following model, termed the integrated velocity and acceleration fusion model, enhances the subject CAV's acceleration determination by incorporating state information from multiple lead and following vehicles. Incorporating graph sample and aggregate-based neural networks, as well as the gated recurrent unit, facilitates the recognition of driving intentions and the prediction of trajectories for surrounding vehicles. Theoretical foundations underpin these models, contributing to their robustness and effectiveness in diverse driving scenarios.

Simulation results demonstrated notable improvements in traffic efficiency, safety, robustness, and scalability when employing LMs for cooperative CAV control. However, it is essential to acknowledge certain limitations in this study. Real-world uncertainties, such as unpredictable traffic conditions or communication delays, may influence the effectiveness of the proposed approach. Additionally, the computational demands of large-scale LMs and the need for extensive training data pose practical challenges. For future work, conducting real-world experiments to validate the proposed algorithms and models under varied and dynamic conditions is imperative.

## REFERENCES

- [1] A. Eskandarian, C. Wu, and C. Sun, "Research advances and challenges of autonomous and connected ground vehicles," *IEEE Trans. Intell. Transp. Syst.*, vol. 22, no. 2, pp. 683–711, Feb. 2021.
- [2] S. Mozaffari, O. Y. Al-Jarrah, M. Dianati, P. Jennings, and A. Mouzakitis, "Deep learning-based vehicle behavior prediction for autonomous driving applications: A review," *IEEE Trans. Intell. Transp. Syst.*, vol. 23, no. 1, pp. 33–47, Jan. 2022.
- [3] Y. F. Ma, Z. Y. Wang, H. Yang, and L. Yang, "Artificial intelligence applications in the development of autonomous vehicles: A survey," *IEEE/CAA J. Automatica Sinica*, vol. 7, no. 2, pp. 315–329, Mar. 2020.
- [4] J. Y. Zhan, Z. B. Ma, and L. G. Zhang, "Data-driven modeling and distributed predictive control of mixed vehicle platoons," *IEEE Trans. Intell. Veh.*, vol. 8, no. 1, pp. 572–582, Jan. 2023.
- [5] M. Noor-A-Rahim et al., "6G for vehicle-to-everything (V2X) communications: Enabling technologies, challenges, and opportunities," *Proc. IEEE*, vol. 110, no. 6, pp. 712–734, Jun. 2022.
- [6] L. Zheng, T. Sayed, and F. Mannering, "Modeling traffic conflicts for use in road safety analysis: A review of analytic methods and future directions," *Anal. Methods Accident Res.*, vol. 9, Mar. 2021, Art. no. 100142.
- [7] G. Schweiger, H. Nilsson, J. Schoeggel, W. Birk, and A. Posch, "Modeling and simulation of large-scale systems: A systematic comparison of modeling paradigms," *Appl. Math. Computation*, vol. 365, Jan. 2020, Art. no. 124713.
- [8] H. Jahanbakhthi, "A novel fractional-order neural network for model reduction of large-scale systems with fractional-order nonlinear structure," *Soft Comput.*, vol. 24, no. 17, pp. 13489–13499, Sep. 2020.
- [9] Y. L. Zheng and Q. S. Liu, "A review of distributed optimization: Problems, models and algorithms," *Neurocomputing*, vol. 483, pp. 446–459, Apr. 2022.
- [10] Y. He, K. Huang, G. Z. Zhang, F. R. Yu, J. Y. Chen, and J. Q. Li, "Bift: A blockchain-based federated learning system for connected and autonomous vehicles," *IEEE Internet Things J.*, vol. 9, no. 14, pp. 12311–12322, Dec. 2021.
- [11] Y. Wang, H. X. Liu, Y. C. Fan, J. X. Ding, and J. C. Long, "Large-scale multimodal transportation network models and algorithms-part II: Network capacity and network design problem," *Transp. Res. Part E: Logistics Transp. Rev.*, vol. 167, Nov. 2022, Art. no. 102918.
- [12] S. Zhao, T. Y. Zhang, M. Hu, W. Chang, and F. C. You, "AP-BERT: Enhanced pre-trained model through average pooling," *Appl. Intell.*, vol. 52, no. 14, pp. 15929–15937, Mar. 2022.
- [13] J. Jeon and S. Y. Lee, "Large language models in education: A focus on the complementary relationship between human teachers and ChatGPT," *Educ. Inf. Technol.*, vol. 28, no. 12, pp. 15873–15892, May 2023.
- [14] S. B. Liu, Q. Z. Lin, K. C. Wong, Q. Li, and K. C. Tan, "Evolutionary large-scale multiobjective optimization: Benchmarks and algorithms," *IEEE Trans. Evol. Computation*, vol. 27, no. 3, pp. 401–415, Jun. 2023.
- [15] M. T. Chao and L. Q. Liu, "A dynamical alternating direction method of multipliers for two-block optimization problems," *Nonlinear Dyn.*, vol. 111, no. 7, pp. 6557–6583, Apr. 2023.
- [16] S. H. Cui, F. Cao, B. Yu, and B. Z. Yao, "Modeling heterogeneous traffic mixing regular, connected, and connected-autonomous vehicles under connected environment," *IEEE Trans. Intell. Transp. Syst.*, vol. 23, no. 7, pp. 8579–8594, Jun. 2022.
- [17] P. Arthurs, L. Gillam, P. Krause, N. Wang, K. Halder, and A. Mouzakitis, "A taxonomy and survey of Edge Cloud computing for intelligent transportation systems and connected vehicles," *IEEE Trans. Intell. Transp. Syst.*, vol. 23, no. 7, pp. 6206–6221, Jul. 2022.
- [18] F. Fakhroosavi, R. Saedi, A. Zockaie, and A. Talebpour, "Impacts of connected and autonomous vehicles on traffic flow with heterogeneous drivers spatially distributed over large-scale networks," *Transp. Res. Rec.*, vol. 2674, no. 10, pp. 817–830, Oct. 2020.
- [19] Z. M. Huang, S. J. Shen, and J. Ma, "Decentralized iLQR for cooperative trajectory planning of connected autonomous vehicles via dual consensus ADMM," *IEEE Trans. Intell. Transp. Syst.*, vol. 24, no. 11, pp. 12754–12766, Nov. 2023.
- [20] S. Y. Gong and L. L. Du, "Cooperative platoon control for a mixed traffic flow including human drive vehicles and connected and autonomous vehicles," *Transp. Res. Part B: Methodol.*, vol. 116, pp. 25–61, Oct. 2018.
- [21] A. Khalil, K. F. Aljanaideh, and M. Al Janaideh, "On connected autonomous vehicles with unknown Human driven vehicles effects using transmissibility operators," *IEEE Trans. Autom. Sci. Eng.*, vol. 20, no. 3, pp. 1876–1889, Jul. 2023.
- [22] J. Wang, S. Peeta, and X. Z. He, "Multiclass traffic assignment model for mixed traffic flow of human-driven vehicles and connected and autonomous vehicles," *Transp. Res. Part B: Methodol.*, vol. 126, pp. 139–168, Aug. 2019.
- [23] Z. Y. Song and H. T. Ding, "Modeling car-following behavior in heterogeneous traffic mixing human-driven, automated and connected vehicles: Considering multitype vehicle interactions," *Nonlinear Dyn.*, vol. 111, no. 12, pp. 11115–11134, Jun. 2023.
- [24] M. Atagoziev, E. G. Schmidt, and K. W. Schmidt, "Lane change scheduling for connected and autonomous vehicles," *Transp. Res. Part C: Emerg. Technol.*, vol. 147, Feb. 2023, Art. no. 103985.
- [25] Y. M. Chen, C. Lu, and W. B. Chu, "A cooperative driving strategy based on velocity prediction for connected vehicles with robust path-following control," *IEEE Internet Things J.*, vol. 7, no. 5, pp. 3822–3832, May 2020.
- [26] H. Ding, Y. R. Di, X. Y. Zheng, H. J. Bai, and W. H. Zhang, "Automated cooperative control of multilane freeway merging areas in connected and autonomous vehicle environments," *Transportmetrica B: Transport Dyn.*, vol. 9, no. 1, pp. 437–455, Jan. 2021.
- [27] G. Thandavarayan, M. Sepulcre, and J. Gozalvez, "Cooperative Perception for connected and automated vehicles: Evaluation and impact of congestion control," *IEEE Access*, vol. 8, pp. 197665–197683, 2020.
- [28] X. X. Zhang, Z. L. Cheng, J. Ma, S. A. Huang, F. L. Lewis, and T. H. Lee, "Semi-definite relaxation-based ADMM for Cooperative planning and control of connected autonomous vehicles," *IEEE Trans. Intell. Transp. Syst.*, vol. 23, no. 7, pp. 9240–9251, Jul. 2022.
- [29] S. Boddupalli, A. S. Rao, and S. Ray, "Resilient cooperative adaptive cruise control for autonomous vehicles using machine learning," *IEEE Trans. Intell. Transp. Syst.*, vol. 23, no. 9, pp. 15655–15672, Sep. 2022.
- [30] J. J. Jiao, H. L. Trentelman, and M. K. Camlibel, "A suboptimality approach to distributed linear quadratic optimal control," *IEEE Trans. Autom. Control*, vol. 65, no. 3, pp. 1218–1225, Mar. 2020.
- [31] A. M. Mirzendehtel and M. Behandish, "Co-design optimization of moving parts for compliance and collision avoidance," *Comput. Aided Des.*, vol. 163, Oct. 2023, Art. no. 103547.
- [32] W. Q. Bai, B. Xu, H. Liu, Y. C. Qin, and C. L. Xiang, "Robust longitudinal distributed model predictive control of connected and automated vehicles with coupled safety constraints," *IEEE Trans. Veh. Technol.*, vol. 72, no. 3, pp. 2960–2973, Mar. 2023.
- [33] E. G. Birgin and J. M. Martinez, "Complexity and performance of an augmented lagrangian algorithm," *Optim. Methods Softw.*, vol. 35, no. 5, pp. 885–920, Sep. 2020.
- [34] L. Wang and B. K. P. Horn, "On the stability analysis of mixed traffic with vehicles under car-following and bilateral control," *IEEE Trans. Autom. Control*, vol. 65, no. 7, pp. 3076–3083, Jul. 2020.
- [35] S. Y. Wang, B. Yu, and M. Y. Wu, "MVCM car-following model for connected vehicles and simulation-based traffic analysis in mixed traffic flow," *IEEE Trans. Intell. Transp. Syst.*, vol. 23, no. 6, pp. 5267–5274, Jun. 2022.
- [36] Y. F. Li et al., "Modeling and simulation for microscopic traffic flow based on multiple headway, velocity and acceleration difference," *Nonlinear Dyn.*, vol. 66, no. 1/2, pp. 15–28, Oct. 2011.
- [37] J. W. Wang, Y. Zheng, K. Q. Li, and Q. Xu, "Deep-LCC: Data-Enabled predictive leading cruise control in mixed traffic flow," *IEEE Trans. Control Syst. Technol.*, vol. 31, no. 6, pp. 2760–2776, Nov. 2023.
- [38] I. M. Abuamer, M. Sadat, M. A. Silgu, and H. B. Celikoglu, "Analyzing the effects of driver behavior within an adaptive ramp control scheme: A case-study with ALINEA," in *Proc. IEEE Int. Conf. Veh. Electron. Saf.*, pp. 109–114, Jun. 2017.

- [39] I. M. Abuamer and H. B. Celikoglu, "Local ramp metering Strategy ALINEA: Microscopic simulation based evaluation study on Istanbul freeways," in *Proc. 19TH Euro Work. Group Transp. Meeting*, Sep. 2016, pp. 598–606.
- [40] V. Embar, S. Srinivasan, and L. Getoor, "A comparison of statistical relational learning and graph neural networks for aggregate graph queries," *Mach. Learn.*, vol. 110, no. 7, pp. 1847–1866, Jul. 2021.
- [41] M. A. Silgu, I. G. Erdagi, G. Goksu, and H. B. Celikoglu, "Combined control of freeway traffic involving cooperative adaptive cruise controlled and Human driven vehicles using feedback control through SUMO," *IEEE Trans. Intell. Transp. Syst.*, vol. 23, no. 8, pp. 11011–11025, Aug. 2022.
- [42] M. A. Silgu, "A framework for evaluating the safety and homogenizing effect of freeway traffic controllers on mixed traffic conditions," *Arab. J. Sci. Eng.*, vol. 49, pp. 4995–5010, Oct. 2023.
- [43] I. G. Erdagi, M. A. Silgu, and H. B. Celikoglu, "Emission effects of Cooperative adaptive cruise control: A simulation case using SUMO," *SUMO User Conf.*, vol. 62, pp. 92–100, Aug. 2019.
- [44] M. A. Silgu, I. G. Erdagi, G. Goksu, and H. B. Celikoglu, " $H_\infty$  State feedback controller for ODE model of traffic flow," *16th IFAC Symp. Control Transp. Syst. (CTS)*, vol. 54, no. 2, pp. 19–24, Jul. 2021.
- [45] M. A. Silgu, I. G. Erdagi, G. Goksu, and H. B. Celikoglu, "Combined control of freeway traffic involving cooperative adaptive cruise controlled and Human driven vehicles using feedback control through SUMO," *IEEE Trans. Intell. Transp. Syst.*, vol. 23, no. 8, pp. 11011–11025, Aug. 2022.
- [46] M. A. Silgu, I. G. Erdagi, and H. B. Celikoglu, "Network-wide emission effects of cooperative adaptive cruise control with signal control at inter-sections," *Transp. Res. Proc.*, vol. 47, pp. 545–552, Apr. 2020.
- [47] J. L. Shen, E. K. H. Kammara, and L. L. Du, "Nonconvex, fully distributed optimization based CAV platooning control under nonlinear vehicle dynamics," *IEEE Trans. Intell. Transp. Syst.*, vol. 23, no. 11, pp. 20506–20521, Nov. 2022.
- [48] S. Goncu, I. G. Erdagi, M. A. Silgu, and H. B. Celikoglu, "Analysis on effects of driving behavior on freeway traffic flow: A comparative evaluation of two driver profiles using two car-following models," in *Proc. IEEE Intell. Veh. Symp.*, Jun. 2022, pp. 688–693.
- [49] V. Milanés and S. E. Shladover, "Modeling cooperative and autonomous adaptive cruise control dynamic responses using experimental data," *Transp. Res. Part C: Emerg. Technol.*, vol. 48, pp. 285–300, Nov. 2014.
- [50] X. X. Wu, H. Lu, K. Li, Z. Y. Wu, X. Y. Liu, and H. L. Meng, "Hiformer: Sequence modeling networks with hierarchical attention mechanisms," *IEEE/ACM Trans. Audio Speech Lang. Process.*, vol. 31, pp. 3993–4003, Nov. 2023.
- [51] J. Li, Y. Bao, W. X. Liu, P. X. Ji, L. K. Wang, and Z. B. Wang, "Twins transformer: Cross-attention based two-branch transformer network for rotating bearing fault diagnosis," *Measurement*, vol. 223, Nov. 2023, Art. no. 113687.
- [52] P. B. Fu, D. X. Liu, and H. R. Yang, "LAS-transformer: An enhanced transformer based on the local attention mechanism for speech recognition," *Information*, vol. 13, no. 5, May 2022, Art. no. 250.
- [53] Y. Y. Yan, F. A. Liu, X. Q. Zhuang, and J. Ju, "An R-Transformer\_BiLSTM model based on attention for multi-label text classification," *Neural Process. Lett.*, vol. 55, no. 2, pp. 1293–1316, Jun. 2022.
- [54] M. J. Ma, H. Y. Xia, Y. M. Tan, H. S. Li, and S. X. Song, "HT-Net: Hierarchical context-attention transformer network for medical CT image segmentation," *Appl. Intell.*, vol. 52, no. 9, pp. 10692–10705, Jan. 2022.
- [55] J. Zeng, Y. Ren, K. Wang, X. Hu, and J. F. Li, "Spatio-temporal-attention-based vehicle trajectory prediction considering multi-vehicle interaction in mixed traffic flow," *Appl. Sci.*, vol. 14, no. 1, Jan. 2024, Art. no. 161.
- [56] S. Tanno, Y. Tamura, and Y. Hirata, "Trajectory prediction considering the behavior of pedestrians intersecting with vehicles," *Adv. Robot.*, vol. 37, no. 18, pp. 1198–1209, Sep. 2023.
- [57] D. X. Sun, H. W. Guo, and W. H. Wang, "Vehicle trajectory prediction based on multivariate interaction modeling," *IEEE Access*, vol. 11, pp. 131639–131650, Dec. 2023.
- [58] S. Y. Qiao, F. Gao, J. H. Wu, and R. Zhao, "An enhanced vehicle trajectory prediction model leveraging LSTM and social-attention mechanisms," *IEEE Access*, vol. 12, pp. 1718–1726, Jan. 2024.
- [59] Z. Y. Zhang, C. Y. Wang, W. Z. Zhao, M. C. Cao, and J. Q. Liu, "Ego vehicle trajectory prediction based on time-feature encoding and physics-intention decoding," *IEEE Trans. Intell. Transp. Syst.*, early access, Jan. 16, 2024, doi: [10.1109/TITS.2023.3344718](https://doi.org/10.1109/TITS.2023.3344718).